Cynarin blocks Ebola virus replication by counteracting VP35 inhibition of interferon-beta production

Angela Corona [a,*], Elisa Fanunza [a], Cristiano Salata [b,c], Melody Jane Morwitzer [d], Simona Distinto [a], Luca Zinzula [e], Cinzia Sanna [a], Aldo Frau [a], Gian Luca Daino [a], Marina Quartu [f], Orazio Taglialatela-Scafati [g], Daniela Rigano [g], StPatrick Reid [d], Alì Mirazimi [c,h,i], Enzo Tramontano [a]

[a] Department of Life and Environmental Sciences, University of Cagliari, 09042, Monserrato, Italy
[b] Department of Molecular Medicine, University of Padova, 35121, Padova, Italy
[c] Department of Microbiology, Public Health Agency of Sweden, SE-171 82, Solna, Sweden
[d] Department of Pathology and Microbiology, 985900 Nebraska Medical Center, Omaha, USA
[e] Department of Molecular Structural Biology, The Max-Planck Institute of Biochemistry, 82152, Martinsried, Germany
[f] Department of Biomedical Sciences, University of Cagliari, 09042, Monserrato, Italy
[g] Department of Pharmacy, University of Naples Federico II, 08131, Naples, Italy
[h] Department of Laboratory Medicine, Karolinska University Hospital and KI, SE-14186, Huddinge, Stockholm, Sweden
[i] National Veterinary Institute, SE-756 51, Uppsala, Sweden

ARTICLE INFO

Keywords:
RNA binding protein inhibitor
Type I IFN antagonist
Viral immune antagonist
Cynarin
Dicaffeolyliquinic acid
Ebola virus VP35
Ebola virus inhibition

ABSTRACT

Ebola virus (EBOV) is one of the deadliest infective agents whose lethality is linked to the ability to efficiently bypass the host's innate antiviral response. EBOV multifunctional protein VP35 plays a major role in viral replication both as polymerase cofactor and interferon (IFN) antagonist. By hiding the non-self 5′-ppp dsRNA from the cellular receptor RIG-I, VP35 prevents its activation and inhibits IFN-β production. Blocking VP35- dsRNA interaction and IFN-β suppression is a validated drug target.

We screened a library of natural extracts and found that cynarin inhibits dsRNA-VP35 binding with an IC_{50} value of 8.5 μM. It reverts the EBOV VP35 inhibition of IFN-β production, while it does not induce IFN production by itself. Docking experiments suggest that the molecule can bind on the end-capping pocket of VP35 C-terminal Interferon Inhibitory domain (IID), and differential scanning fluorimetry confirmed that cynarin interacts with VP35-IID with a K_D of 12 μM. Cynarin was further tested in an EBOV minigenome assay but did not inhibit VP35 polymerase cofactor activity. When evaluated during challenge of IFN-susceptible A549 cells with EBOV isolate derived from the 2014 West African outbreak, cynarin was able to inhibit viral replication with an EC_{50} value of 9.1 μM, showing no significant cytotoxicity.

Our findings show that cynarin blocks EBOV replication by acting directly on VP35 and subverting its IFN antagonism function but not cofactor function, and as such identify the first EBOV inhibitor with this mode of action.

1. Introduction

Ebola virus (EBOV) was first discovered in 1976 near the Ebola river in Zaire (now Democratic Republic of the Congo (DRC)) (Johnson, K et al., 1977) as the etiological agent of a highly lethal hemorrhagic fever, now termed Ebola virus disease (EVD). EVD has re-emerged in the last decade with an increase of incidence and geographical extension of human outbreaks. In 2021 two outbreaks stared in DRC and Guinea, increasing the concern of endemization of the virus in West-Africa, and were both declared over in May and June respectively (World Health Organization, 2019) .

Treatments for EVD have long been limited, however the Food and Drug Administration (FDA) recently approved Erbevo, a recombinant vesicular-stomatitis virus-based vaccine (Ollmann Saphire, 2020), and

* Corresponding author.
E-mail address: angela.corona@unica.it (A. Corona).

inmazeb (FDA 2020), a monoclonal antibody cocktail that targets the EBOV glycoprotein (FDA, 2020). Administered by intravenous infusion, inmazeb is effective but has several limitations due to availability, adverse effects, and cost. Moreover, the persistence of residual virus in survivors is well documented, leading to long-term sequelae that would require a more systematic chronic treatment (Malvy et al., 2019). Therefore, efforts are devoted to explore all the possible targets and mechanisms for the development of new anti-EBOV therapeutics that are more versatile and cost-effective (Fanunza et al., 2019).

The EVD onset is linked to the ability of EBOV to efficiently suppress the innate immune system at the early stages of infection (Mahanty and Bray, 2004). Moreover, pharmacological amplification of the innate immune response has been shown to overcome EBOV replication (Jasenosky et al., 2019). The multifunctional proteins VP35 plays a leading role in EBOV innate immune evasion, being a main determinant of EBOV virulence (Leung et al., 2010a; Prins et al., 2010b).

The VP35 suppression of the IFN—α/β production is exerted by preventing the activation of the retinoic acid-inducible gene I (RIG-I)- like receptor by sequestering double-stranded RNA (dsRNA) (Cardenas et al., 2006), intermediate of viral replication, so hiding its presence, and also inhibiting the RIG-I cascade at several levels (Fanunza et al., 2018a; Messaoudi et al., 2015): (i) interacting with RNA-activated protein ki- nase (PKR) activator (PACT) to disable its interaction with RIG-I (Leung et al., 2010a; Luthra et al., 2013); (ii) interacting with TBK-1 and IKKε (Prins et al., 2009) to block their interactions with their substrate IRF-3;
(iii) interacting with both IRF-3 and IRF-7 to promote their SUMOyla- tion (Chang et al., 2009), hence inhibiting TRIM6-mediated type I IFN production (Bharaj et al., 2017), and (iv) repressing the stress granule assembly (Le Sage et al., 2017; Nelson et al., 2016).

Moreover, similar to its orthologous counterpart in the *Mononegavirales* order, VP35 is a key component of the viral polymerase complex (Mühlberger et al., 1999). Specifically, VP35 serves as bridge between the viral RNA-dependent RNA polymerase (L) and the nucleoprotein (NP) (Leung et al., 2015), it is involved in viral genome packaging and nucleocapsid formation (Takamatsu et al., 2018) and recently it has been shown to possess NTPase and helicase-like activities poten- tially involved in viral RNA remodeling (Shu et al., 2019).

Interestingly, Woolsey et al. demonstrate that immune evasion functions of the EBOV VP35 protein are critical for virulence in non-human primates (Woolsey et al., 2019). A VP35 mutant EBOV does not cause lethal disease and instead elicits adaptive immune responses that can protect animals from wild-type EBOV challenge. Therefore, given its multifunctional nature and its numerous roles in EBOV infec- tion and pathogenesis, VP35 has been validated as a major target for drug development against EBOV (Daino et al., 2018; Fanunza et al., 2018a, 2019; Iversen et al., 2012; Mitchell and Carter, 2014; Seesuay et al., 2018a).

VP35 is a 340 amino acid protein that contains three main functional domains: the N-terminus possesses an NP-chaperoning domain that regulates capsid assembly and genome binding (Kirchdoerfer et al., 2015) as well as a homo-multimerization domain (Di Palma et al., 2019; Ramaswamy et al., 2018; Zinzula et al., 2019) that is required for full IFN antagonism and is responsible for binding the viral polymerase L (Moller et al., 2005; Reid et al., 2005), and also was suggested to be involved in the inhibition of B cell function and differentiation (Lubaki et al., 2016), proving to be involved also in adaptive and innate cell-mediated responses; the C-terminus contains a dsRNA binding/IFN inhibitory domain (RBD/IID) (Cardenas et al., 2006; Groseth et al., 2009; Leung et al., 2009, 2010b). It has been shown that VP35 binds dsRNA as a dimer wrapping the 3P-dsRNA termini with an asymmetric backbone and end-capping mode: one monomer interacts with the dsRNA terminal bases, while the second one interacts with the nucleic acid phosphate groups (Leung et al., 2010c). Preservation of the IID structure is known to be critical for EBOV, since IID mutations have been shown to suppress the ability of VP35 to bind to dsRNA and further resulted in loss of its IFN antagonism function (Cardenas et al., 2006) as well as its ability to suppress RNA silencing (Haasnoot et al., 2007), and to significant increases in the percentages of phenotypically distinct B-cell subsets and plasma cells (Lubaki et al., 2016) decreasing the viral growth rate and attenuating the virulence in animal models (Woolsey et al., 2019).

Furthermore, analysis of the genetic variations that occurred in the 2014 epidemic revealed that the IID contains a highly conserved α—β basic patch important for dsRNA binding in a sequence-independent manner (Gire et al., 2014; Leung et al., 2009; Prins et al., 2010a), making the ability of VP35 to bind viral dsRNA a key target in EBOV drug discovery (Fanunza et al., 2018a, 2019). In fact, previous investigations of the VP35 IID led to the identification of small molecules and RNA aptamers that disrupt the interaction between VP35 and the viral NP, targeting its polymerase cofactor function (Binning et al., 2013). In the past years, the possibility to target VP35—dsRNA interaction has also been explored by computational techniques (Binning et al., 2013; Shah et al., 2015). Among the identified compounds, one was shown to inhibit the IID VP35—dsRNA interaction with an IC_{50} of 4 μM (Glanzer et al., 2016). Recently, a set of antibody fragments selected by phage display technology significantly decreased the inhibition of RIG-I signaling by VP35 in a cellular system (Flego et al., 2019). A set of transbodies designed to specifically recognize the IID function of VP35 (Seesuay et al., 2018b) were shown to interact with residues important for the VP35-dsRNA binding, such as Arg322 and Lys339, involved in the backbone binding, and residues Ser272, Cys275, Ile278, Gln279 and Ile340, involved in the end-capping, respectively, together with other newly-identified critical residues (Glu269, Gln270, and Asp271) (Seesuay et al., 2018b). This led to the suppression of IFN inhibitory function of VP35 and was responsible for host innate immunity rescue. Recently, we optimized a method that utilizes a fluorescent dsRNA oligomer ligand and showed that the flavonol myricetin is able to suppress the VP35-dsRNA binding with an IC_{50} value of 2.7 μM (Daino et al., 2018). We further developed a gene-reporter assay (56) to determine VP35 inhibition of the RIG-I pathway, which was shown to be reversed by an extract from the leaves of *Asphodelus microcarpus* (57). Thus, natural extracts have been shown to be a useful source of bioactive molecules in the search for anti-EBOV therapeutics.

2. Material and methods

2.1. Extracts and isolate compounds from Onopordum illyricum L

Plant material was processed and isolated compounds were obtained and identified as reported in (Sanna et al., 2018).

2.2. EBOV rVP35 production

A recombinant full-length EBOV VP35 protein from Zaire species (1976 Yambuku-Mayinga strain) containing a N-terminal His6-tag-was subcloned in a pET45 b vector (Novagen) (Zinzula et al., 2009)and produced as previously described (Daino et al., 2018). Briefly, BL21AI *E. coli* were transformed with 200 ng of pET45b-EBOV-VP35 plasmid. Transformants were grow on LB medium containing 150 μg/ml ampicillin at 37 °C, 200 rpm until 0.6 OD_{600}. Protein expression was induced adding 0.4% (w/v) L-arabinose and 0.65 mM Isopropil-β-D-1-tiogalattopiranoside, and culture was incubated ON at 200 rpm at 18 °C. After incubation, the cell culture was centrifuged at 4500×*g* at 4 °C for 20 min and bacterial pellets were collected and frozen at —80 °C. The bacterial pellet was resuspended in 5:1 ml of lysis buffer (100 mM sodium phosphate pH 8.0, 500 mM NaCl, 1 mM 2-mercaptoethanol, 10% glycerol, 20 mM imidazole, 6 M urea). The suspen- sion was incubated on ice for 15 min and subsequently sonicated on ice. The cell lysate was centrifuged at 32,000×*g* at 4 °C for 45 min. The purification was performed in a BioLogic LP Chromatographic System (Biorad). Supernatant was loaded (0.5 ml/min) to an Econo Column (Biorad) packed with 3 ml of Ni-Sepharose High Performance (GE

Healthcare), pre-equilibrated in binding buffer (100 mM sodium phosphate pH 8.0, 300 mM NaCl, 1 mM 2-mercaptoethanol, 10% glycerol, 20 mM imidazole, 6 M urea). Urea content was gradually removed from the column by a decreasing gradient of concentration from 6 up to 0 M with a flow rate of 0.5 ml/min for around 130 column volumes (800 min). The column was washed for 40 column volumes with three Washing buffers (50 mM sodium phosphate pH 8.0, 300 mM NaCl, 1 mM 2-mercaptoethanol, 10% glycerol) with increasing concentrations of imidazole (70 mM–150 mM - 250 mM). Refolded recombinant protein was eluted using 90 ml of the same buffer having 1 M imidazole and fractions collected. Significant eluted fractions, selected on IMAC chromatogram, were analyzed in a 12% SDS–PAGE. Fractions contain- ing pure rVP35 protein were gathered and dialyzed against Dialysis buffer (50 mM sodium phosphate pH 8.0, 800 mM NaCl, 1 mM 2-mer- captoethanol, 10% glycerol). Afterwards, protein concentration was determined by Bradford assay with the Protein Quantification Kit-Rapid (Fluka – Sigma Aldrich).

2.3. Fluorescence-based VP35-RNA interaction assay

A fluorescence-labeled dsRNA oligomer of 30 bp in length and an unlabeled 30 bp oligomer were prepared by annealing from three different ssRNA purchased from Metabion International AG (Germany). Sequences purchased were: a) 5′-ppp-cccuuuccuccuuccuuuuguuccu-cuccc-3′, b) 5-gggagaggaacaaaaggaaggaggaaaggg-3′, c) 5′-Fluorescein-gggagaggaacaaaaggaaggaggaaaggg-3’. Annealing has been conducted in order to have in each dsRNA molecule one 5′-triphosphate end. The integrity of DNA templates, IVT dsRNAs and synthetic dsRNA molecules were assessed by agarose-gel electrophoresis. Nickel-coated plates assay.

In a Pierce® Nickel Coated Plate (Thermo Fisher) the amount of rVP35 needed to saturate Nickel-coated plate well binding capacity (700 ng) was added in each well in a volume of 200 μl of coating buffer (final concentration 50 mM Sodium Phosphate pH 7.5, 150 mM NaCl) and incubated for 30 min at 4 °C under rotating agitation (120 rpm), then washed twice with 200 μl of washing buffer (50 mM Sodium Phosphate pH 7.5, NaCl 150 mM, 0.03% Tween-20). After removing supernatant, a volume of 100 μl was added with 7.5 nM of 30 bp 5′-fluorescein-dsRNA in a reaction mixture having 50 mM Sodium Phosphate pH 7.5, 100 mM NaCl, 20 mM $MgCl_2$, 0.03% Tween-20. When extracts and compounds were tested, different serial dilutions of extracts or compounds were added together with the 30 bp 5′-fluorescein-dsRNA and a short dsRNA oligomer was used as positive control for the inhibition. The plate was incubated for 60 min at 37 °C (200 rpm). After the incubation, unbound dsRNA was removed by two washing with 200 μl of a reaction mixture and then, adding 200 μl of the same buffer, fluorescence signals of samples were read with the above-mentioned plate reader (Victor 3 -Perkin-Elmer). IC_{50} values were determined by GraphPad Prism 6.01.

2.4. Molecular modelling

2.4.1. Ligand preparation

Cynarin has been docked in its global minimum energy conformation as determined by molecular mechanics conformational analysis performed with Macromodel software (Mohamadi et al., 1990). The pro- tocol consisted of 2500 steps with an energy window for saving structure of 10 kJ/mol. The algorithm used was the Monte Carlo method with MMFFs (Merck molecular force fields) (Halgren, 1996) water implicit solvation model and the Polak-Ribier Conjugate Gradient (PRCG) method, converging gradient with a threshold of 0.01 kJ (mol·Å)-1 (Hasel et al., 1988).

2.4.2. Protein preparation

The protein structure was obtained from the PDB web site with pdb code 3L25 (Leung et al., 2010b) The protein was prepared by using the protein preparation wizard protocol included in Schro¨dinger Suite LLC 2018.

2.4.3. Blind docking experiments

Docking experiments were conducted by applying Glide XP (Friesner et al., 2006) QMPL-XP (Cho et al., 2005) and AutoDockVina (Trott and Olson, 2010) docking programs. All settings were left as default. Only for AutodockVina exhaustiveness has been increased to 32 (Daino et al., 2018). The whole VP35 IID was considered in the docking experiments in order to identify the preferred binding site Depictions were taken by means of Pymol,Schro¨dinger LLC, 2014; version 1.7.2.1, and Maestro GUI, Schrodinger LLC. Maestro GUI. New York, NY: Schrodinger LLC; 2018.

2.5. Miniaturized differential scanning fluorimetry (Nano-DSF)

For Nano-DSF experiments, recombinant EBOV VP35 constructs comprising either the IID (residues 147–340) or the oligomerization domain (OD) (residues 75–185) were cloned, expressed and purified as previously described (Zinzula et al., 2009, 2019), then diluted at 0.3 mg/mL in 25 mM Tris, pH 7.4; 150 mM NaCl. Protein was incubated at room temperature for 60 min in the presence of Cynarin at different concentrations (1500–1 μM) and then subjected to unfolding by thermal denaturation using a NanoTemper Prometheus NT.48 DSF instrument. The protein intrinsic fluorescence at 330 and 350 nm was measured over a 20–95 °C temperature gradient on a 0.5 °C/min ramp, and the first derivative of the 330/350 nm fluorescence ratio curve was used to determine the transition points indicative of the protein melting temperature (Tm) values. The compound Myricetin (100 μM) was used as a positive control for the interaction with VP35 IID, EBOV VP35 OD in the presence of Cynarin (100 μM) was used as a negative control. Determination of the dissociation constant describing the VP35 affinity for the two compounds was performed according to Vivoli et al. (2014), by using the sequential binding cooperative model as the one best fitting with the experimental data as well as with known VP35-dsRNA bimodal interaction (Kimberlin et al., 2010). Samples were tested in triplicates or quadruplicates and Tm values were averaged from at least three independent experiments.

2.6. Cells and reagents

HEK293T cells were grown in Dulbecco’s modified Eagle’s medium (Gibco) supplemented with 10% fetal bovine serum (Gibco) and 1% penicillin/streptomycin (Sigma). Cells were incubated at 37 °C in a humidified 5% CO2 atmosphere. Plasmid pGL-IFN-β-luc was kindly provided by Prof Stephan Ludwig, Institute of Molecular Virology, University of Münster, Germany). pRL-TK was purchased form Promega (Promega Italia S.r.l. Milan, Italy). pcDNA3-EBOV VP35, carrying EBOV VP35 gene form Zaire species (1976 Yambuku-Mayinga strain) was constructed as previously reported (Cannas et al., 2015). T-Pro P-Fect Transfection Reagent was from T-Pro Biotechnology. Lipofectamine 3000 was from Thermo Fisher Scientific. D-luciferin and Coelenterazine were purchased form Gold Biotechnology (U.S. Registration No 3,257, 927). Primers were purchased from Metabion (Planegg, Germany). Viral RNA (vRNA) was produced in A549 cells, infected with IAV/Puerto-Rico/8/34 (IAV PR8) strain with a multiplicity of infection of 5. Five hours after infection, total RNA was isolated using the RNeasy Kit (Qiagen). TRIzol™ Reagent was from Thermo Fisher Scientific.

2.7. Luciferase reporter gene assay for interferon promoter activation

Luciferase Reporter Gene Assay was adapted from (Fanunza et al., 2018b, 2020). HEK293T Cells (1.5×10^4 cells/well) were seeded in 96-well plates 24 h before transfection. Cells were transfected using T-Pro P-Fect Transfection Reagent, according to the manufacturer’s protocol. Plasmids (pGL-IFN-β-luc 60 ng; pRL-TK 10 ng plus pcDNA3 VP35 or pcDNA3, pcDNA3 was used as empty vector (EV) in controls)

were mixed with the transfection reagent in reduced serum medium Optimem (Gibco) and incubated 20 min at room temperature. Transfection complexes were then gently added into individual wells of the 96-well plate. Twenty-four hours after transfection, cells were stimu- lated with IAV-RNA (obtained as previously reported (Cannas et al., 2015)), pre-mixed with the transfection reagent in reduced serum medium Optimem, and incubated for 24 h at 37 °C in 5% CO2. Cells were harvested with lysis buffer (50 mM Na-MES [pH 7.8], 50 mM Tris-HCl [pH 7.8], 1 mM dithiothreitol, and 0.2% Triton X-100). To lysates were added luciferase assay buffer (125 mM Na-MES [pH 7.8], 125 mM Tris-HCl [pH 7.8], 25 mM magnesium acetate, and 2.5 mg/mL ATP). Immediately after addition of 50 µl of Luciferin buffer (25 mM D-luciferin, 5 mM KH_2PO_4) the luminescence was measured in Victor3 luminometer (PerkinElmer), and again after addition of 50 µ of Coelenterazine assay buffer (125 mM Na-MES [pH 7.8], 125 mM Tris-HCl [pH 7.8], 25 mM magnesium acetate, 5 mM KH_2PO_4 and 10 µM Coelenterazine). The relative light units (RLU) of Luciferase signal were normalized to Renilla Luc and over unstimulated controls. Each assay was performed in triplicate. Results were expressed in percentage of IFN induction over the empty vector (indicated as 100%) and plotted in mean plus standard deviation of two replicates with GraphPad Prisme 6.01. Data were analyzed with *t*-test.

2.8. Luciferase reporter gene assay for interferon promoter activation

Luciferase Reporter Gene Assay was adapted from (Fanunza et al., 2018b, 2020). HEK293T Cells (1.5×10^4 cells/well) were seeded in 96-well plates 24 h before transfection. Cells were transfected using T-Pro P-Fect Transfection Reagent, according to the manufacturer's protocol. Plasmids (pISRE-luc 70 ng; pRL-TK 10 ng plus 30 ng pcDNA3.1VP24 flag or pcDNA3.1 used as empty vector (EV) in controls) were mixed with the transfection reagent in reduced serum medium Optimem (Gibco) and incubated 20 min at room temperature. Transfection complexes were then gently added into individual wells of the 96-well plate. Twenty-four hours after transfection, cells were stimulated with interferon alpha (37 ng/ml), and compound and incubated for 24 h at 37 °C in 5% CO_2.

Cells were harvested and lysed as reported in 2.7. Each assay was performed in triplicate. Results were expressed in percentage of ISRE-induction over the empty vector (indicated as 100%) and plotted in mean plus standard deviation of two replicates with GraphPad Prisme 6.01. Data were analyzed with *t*-test.

2.9. Immunofluorescence

For immunostaining, HEK293T cells were seeded in 6-well plates (3 x 10^5 cell/well) and cotransfected with Lipofectamine 3000 transfection reagent (Invitrogen) with 2.5 µg/well of pcDNA3 or plasmids for EBOV VP35 protein. After 24 h of transfection, the stimulated sample cells were transfected with 1 µg of vRNA with or without 11 µM Cynarin. 24 h later cells were fixed with 4% paraformaldehyde in PBS for 15 min at RT. Permeabilization was performed with 0,25% Triton X-100 in PBS for 10 min, followed by three washes of 5 min each with PBS, and incu- bation with blocking buffer (5% bovine serum albumin in 0,25% Triton X-100 in PBS) for 1 h at RT. The cells were then incubated with the rabbit anti-Flag (1:500) and goat anti-IRF 3 ser396 (ABIN742688) polyclonal primary antibodies, diluted 1:200 in PBS, for 3 h at RT. After three washes with PBS, cells were incubated with Alexa Fluor 488 conjugated anti-rabbit and Alexa Fluor 594 conjugated anti-goat sera (Invitrogen), both diluted 1:400, used as secondary antibodies, for 1 h at RT and then incubated with the nuclear stain Hoechst (Thermo Fischer Scientific) for 1 min at RT. Immunostained cells were mounted on glass slides with Glycerol Mounting Medium containing 1,4-Diazabicyclo [2.2.2]octane (DABCO) (Sigma-Aldrich) as anti-fade reagent, and observed with an Olympus BX61 microscope, equipped with epifluor- escence illumination. Digital images were captured with a Leica DF 450C camera. The cultures were examined at 40× magnification.

2.10. RT-qPCR assay for ISG expression

HEK293T Cells (3×10^5 cells/well) resuspendend Dulbecco's modified Eagle's medium supplemented with 10% fetal bovine serum were seeded in 6-well plates, pre-treated with 500 µl of Poly-D-lysine hydrobromide 100 µg/ml for 1 h. After 24 h cells were transfected with 2500 ng of plasmid (pcDNA3 VP35, pcDNA3 was used as empty vector (EV) in controls) using Lipofectamine 3000 transfection reagent, according to the manufacturer's protocol. Twenty-four hours after transfection, cells were stimulated with 2500 ng of IAV-RNA, pre-mixed with the transfection reagent in reduced serum medium Optimem, and incubated for 24 h at 37 °C in 5% CO2. Total RNA was extracted from transfected cells with TRIzol® Reagent (Invitrogen). RNA was then reverse transcribed and amplified using Luna Universal One-Step RT-qPCR kit (New England Biolabs). Quantitative real-time PCR (RT-qPCR) experiments were performed in triplicate in a CFX-96 Real-Time system (Biorad). Primers used: GAPDH Forward 5′-GAGTCAACG-GATTTTGGTCGT-3′, GAPDH Reverse 5′-TTGATTTTGGAGGGATCTCG-3'; ISG15 Forward 5′-TCCTGGTGAGGAATAACAAGGG-3'; ISG15 Reverse 5′-CTCAGCCAGAACAGGTCGTC-3'; 2′ 5′ OAS Forward 5′-AGCTTCATGGAGAGGGGCA-3'; 2′5′OAS Reverse 5′-AGGCCTGGCT-GAATTACCCAT-3'. Data were analyzed with Opticon Monitor 3.1. mRNA expression levels were normalized to the level of glyceraldehyde-3-phosphate dehydrogenase (GAPDH). Results were expressed in percentage of gene expression over the empty vector (indicated as 100%) and plotted in mean plus standard deviation of two replicates with GraphPad Prisme 6.01.

2.11. Cell viability assay

The cytotoxic activity of compounds on HEK293T was determined according to the protocol used to assess the effect on IFN promoter activation HEK293T cells (1.5×10^4 cells/well) were seeded in 96-well plates. Forty-eight hours after seeding, cells were treated with compounds at increasing concentrations. Twenty-four hours after compound treatment, 10 µL/well of PrestoBlue Cell Viability Reagent (Thermo Fisher Scientific) was added. Plates were then incubated for 60 min in the dark, followed by fluorescence reading at 530 nm/590 nm (excitation/emission wavelength).The cytotoxic activity of compound on A549 cells was determined on exponentially growing cells in complete medium at 24 h and 48 h. Cells were plated in quadruplicate at a density of 1 x 10^4 cells per well, in 96-well plate. On the following day compounds were added to the experimental final concentrations in fresh medium. 24 h and 48 h later, cells were incubated with MTT dye (Cell Proliferation Kit I, Roche Life Science) according to the manufacturer's instructions. Optical density was determined by measuring absorbance at 550 nm and 650 nm.

2.12. EBOV minigenome replication

A RNA polymerase II-driven EBOV minigenome was used as previously described (Nelson et al., 2017). Briefly, HeLa cells (3.0×10^5) were seeded in 100 mm plates 24 h before transfection. Cells were transfected with minigenome components (1.25 µg pCAGGS-HA-NP, 1.25 µg pCAGGS-FLAG-VP35, 0.5 µg pCAGGS-V5-VP30, 0.5 µg pCAGGS-L, and 7.5 µg of pCAGGS-3E5E-luciferase) along with 0.5 µg pRL-TK (for transfection efficiency control) using jetPRIME reagent (Polyplus-transfection (S.A., Illkirch, France)) as per manufacturer's recommendation. For the no L control, total DNA levels were kept constant by complementing transfections with empty-vector pcDNA3. Six hours post-transfection, cells were trypsinized and seeded in 96-well tissue culture plates at 4.0 x 10^4 cells/well with no treatment (L) or with the indicated compounds: DMSO vehicle control (VC), ribavirin (5, 25, 50 µM), or Cynarin (0.1, 0.3, 1, 3, 10, 30 µM).

Reporter activity was measured 24 h post-transfection using the Dual-Glo Luciferase Assay System and a Tecan Spark microplate luminometer (Tecan Trading AG, Switzerland). To account for potential differences in transfection efficiency, firefly luciferase activity was normalized to Renilla luciferase values and plotted as fold activity calculated relative to the no L control. Mean ± standard error of the mean (SEM) values were calculated using GraphPad Prism 7.05 software.

2.13. EBOV stock preparation

All of the EBOV experiments were conducted at the BSL-4 laboratory in Stockholm, Sweden. EBOV (Ebola virus/H.sapiens-tc/SLE/2014/Makona) (Rosenstierne et al., 2016) was grown in Vero cells, and then serially 10-fold diluted in DMEM with 2% FBS inactivated and titrated on Vero cells in 96-well plates. After 24 h incubation, cells were fixed with methanol-acetone and stained by immunofluorescence assay using a rabbit polyclonal anti-EBOV-GP antibody (Rosenstierne et al., 2016) and an Alexa Fluor® 488-conjugated Antibody, according to the manufacturer's instructions. The fluorescent foci in each well were counted and viral titer was expressed as Fluorescence Focus Units (FFUs) per mL (Weidmann et al., 2011).

2.14. Test of inhibition of EBOV infection

Evaluation of anti-Ebola virus activity of the cynarin. A549 cells (1.2×10^4) were seeded in 96 well plates. Twenty-four hours after, cells were infected with roughly 0.005–0.05 FFU/cell of virus in the presence of the appropriate compound concentration (Cynarin 1, 5, 10, 25, 50 μM or IFN-α 2000 IU/mL) and analyzed after 48 h (Salata et al., 2015). Cells were then fixed and stained for the presence of the EBOV-GP protein as reported above. Count of GP-positive cells/well was performed and data (mean ± SD) were reported as are percentage of Ebola virus infected cells (GP positive cells) with respect to DMSO vehicle treated cells, set as 100%.

3. Results

3.1. Onopordum Illyricum components inhibit EBOV VP35 interaction with dsRNA

The total extract from *Onopordum illyricum* was tested for its ability to inhibit dsRNA/VP35 interaction using as a positive control a dsRNA of 30 bp (50 nM). To identify VP35 ligands, we used a full length recom- binant VP35 (rVP35) (Zinzula et al., 2009, 2012) instead of the heavily truncated version (amino acids 171–339) used in other studies (Carde- nas et al., 2006). Since the integral structure of VP35 is needed for maximal suppression of IFN production (Moller et al., 2005; Reid et al., 2005), this maximizes the possibilities of identifying optimal candidates for inhibition of EBOV replication in Biosafety level 4 (BSL4) experi- ments. Results showed that the total *Onopordum illyricum* extract inhibited ds-RNA/rVP35 binding with an IC_{50} value of 26.9 ± 3.3 μg/ml (Fig. 1A). In order to find the constituents responsible for this activity, the extract was chromatographed and the fractions, obtained by eluting with solvents of increasing polarity, were tested and shown to inhibit dsRNA-rVP35 binding with IC_{50} around 30 μg/ml (Fig. 1B). When analyzed for their main components, seven constituents were purified by HPLC (Fig. 2). Among them were two germacrane sesquiterpenes 8α-(5′-hydroxyangeloyl)-salonitenolide (HAS) and onopordopicrin; three chromone derivatives hispidulin, luteolin and apigenin, and arctiine and cynarin. The compounds were first tested at 100 μM against the dsRNA-VP35 interaction, and the two most active components were cynarin and HAS, that inhibited 90% and 60%, respectively, of the VP35-dsRNA binding (Fig. 1C). To better characterize their effects, we determined that their IC_{50} values were 8.5 μM and 77 μM for cynarin and HAS, respectively (Fig. 1D). Cynarin was therefore chosen as lead compound for further characterization.

3.2. Cynarin binds EBOV VP35 IID domain

In order to obtain insights into the cynarin mode of interaction, blind docking experiments were carried out considering one of the available

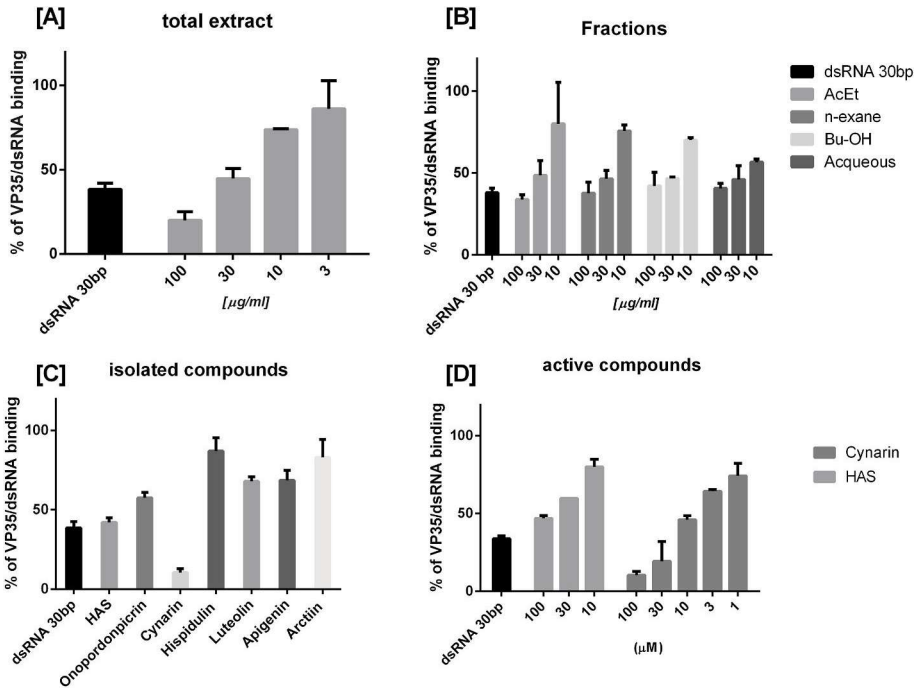

Fig. 1. Inhibition of EBOV VP35 binding to dsRNA [A] *Onopordum Illyricum* total extract [B] and fractions; [C] isolated compounds; [D] and most active compounds. Results were expressed in folds of induction over unstimulated control transfected with the empty vector and plotted in mean plus standard deviation of two independent experiments on duplicate, with GraphPad Prisme 6.01.

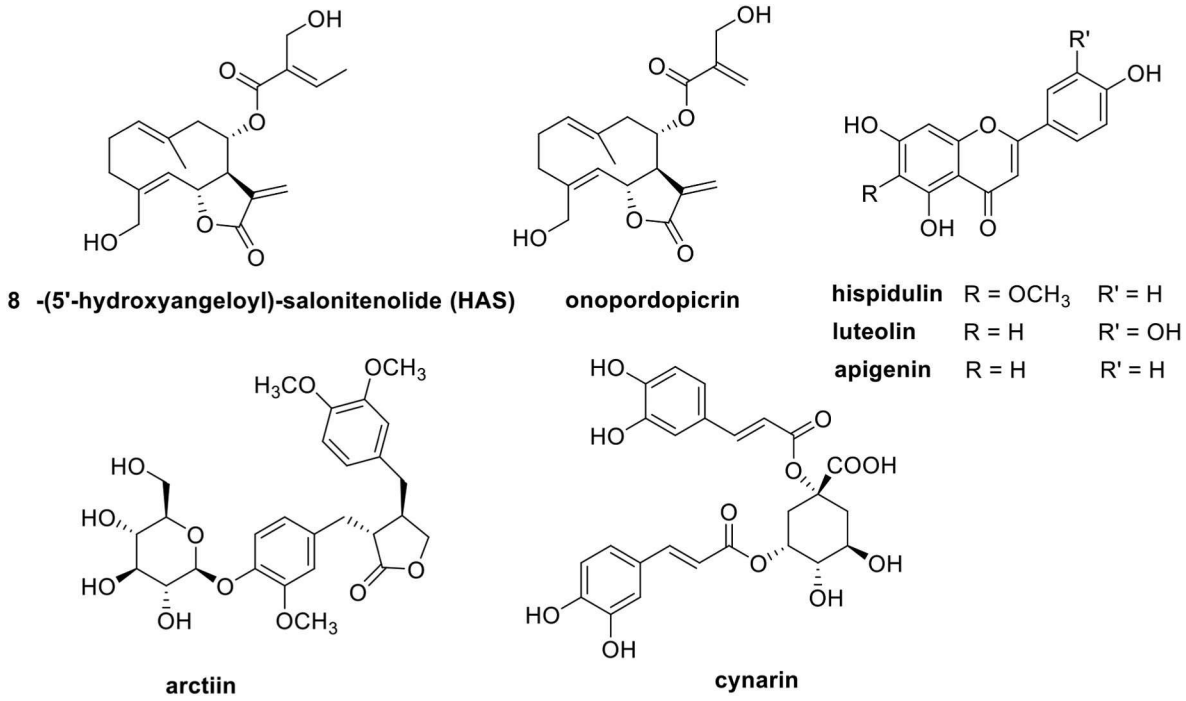

Fig. 2. Chemical structures of the components isolated from O. Illyricum extract.

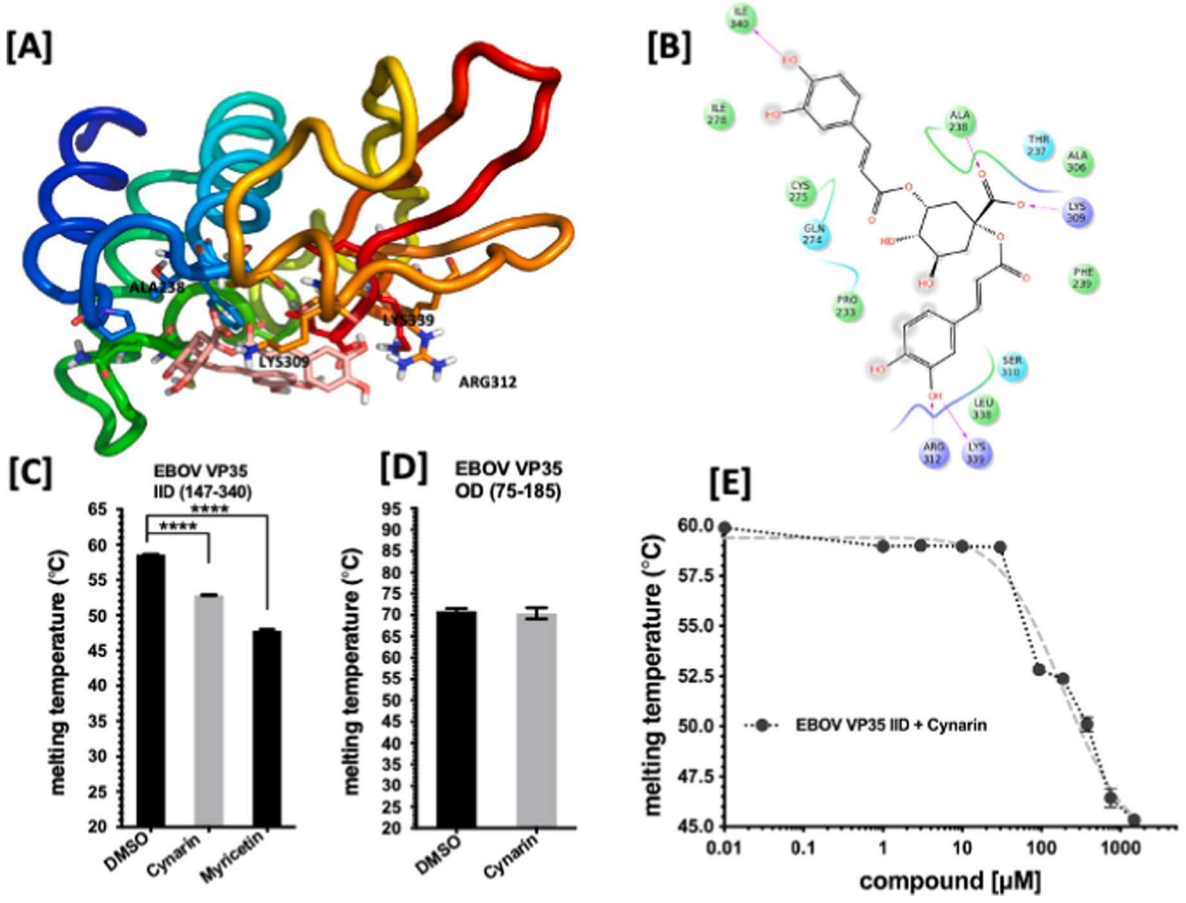

Fig. 3. Cynarin interaction with IID of EBOV VP35. Putative binding mode cynarin (pink sticks) in complex with VP35 IID [A]. [B] 2D depictions of interactions of cynarin -VP35 IID complex. [C] VP35 IID Tm values obtained in presence of DMSO or 100 μM compound concentration. [D] VP35 OD Tm values obtained in presence of DMSO or 100 μM compound concentration [E] Non-linear regression fitting curve of cynarin titration to VP35 IID as a function of Tm. (For interpretation of the references to colour in this figure legend, the reader is referred to the Web version of this article.)

crystal structures of the EBOV VP35 IID domain that is involved in dsRNA binding (Leung et al., 2010b). To increase confidence on the suggested binding mode, a consensus docking approach was considered: three molecular docking algorithms were applied, and the best poses of the active compound were analyzed and compared. The putative bind- ing mode suggested by all algorithms was similar. All programs gave the end-capping binding as the preferred one (Fig. 3A). In order to validate this interpretation, the interaction between VP35 IID and cynarin was evaluated by Differential Scanning Fluorimetry (Nano-DSF) (Fig. 3D). Results showed that the compound cynarin binds to VP35 IID and causes local structural perturbations that affect the protein thermal stability and/or increases its flexibility, lowering the protein Tm by 6 °C with respect to wild-type VP35. By contrast, Cynarin did neither bind nor affected the thermal stability of EBOV VP35 OD, which correlates with the specificity of the compound interaction with the VP35 region involved in dsRNA binding (Fig. 3D). Myricetin, which lowers the Tm of EBOV VP35 IID by 10.8 °C (Fig. 3C) was used as positive control. When a titration of the effect was conducted, cynarin showed an apparent K_D value within the 10–30 μM range (Fig. 3E).

3.3. Cynarin reverts the EBOV VP35 block of IFN-β promoter activation

To evaluate if the cynarin binding to the VP35 IID could revert the VP35 inhibition of the RIG-I pathway, we first sought to test the compound on a luciferase gene-reporter assay to quantify the activation of the IFN-β promoter. The potential cytotoxic effect was preliminarily evaluated, using as a comparison the total extract and the HAS. Cynarin exhibited a CC_{50} value of 113 μM, while both the total extract and HAS showed a CC_{50} value above 300 μM (Fig. 4A). We evaluated their effect on the VP35 inhibition of the INF-β production, upon stimulation with viral RNA (vRNA). Since VP35 acts in a sequence independent manner IAV RNA obtained in house form IAV infection (Cannas et al., 2015) was used to activate the IFN-beta production.Results showed that both the total extract and the cynarin were able to significantly subvert the VP35 block of the IFN-β production (by 49,6% and 50,4% respectively (Fig. 4B). To verify if the cynarin effect was VP35-dependent, we tested the compound in the IFN-β gene reporter assay without VP35 in a dose-response curve and used the same compound concentrations to test the compound in the system with VP35 (Fig. 4C and D). The 100 μM concentration was excluded due to the cytotoxic effect previously observed. The results demonstrated that cynarin did not induce or block IFN production by itself. When tested in stimulated condition, cynarin inhibited IFN-β promoter activation at 33 μM, probably because of residual cytotoxic effect, while it was slightly but not significantly boost- ing the IFN-β promoter activation al lower concentrations (Fig. 4C). Finally, when tested on IFN-β promoter activation in presence of VP35, cynarin treatment was able to revert the VP35 inhibitory effect by 66, 35% at 11 μM (p value = 0,0067) and by 39,5% at 3,7 μM, with an EC_{50} value of 6,6 μM (Fig. 4D).

In order to exclude an effect on other EBOV mechanisms involved in innate immune suppression, cynarin was also tested on the EBOV VP24 inhibition of ISRE promoter activation using the VP24 inhibitor quer- cetin (Fanunza et al., 2020) as a positive control. Results show that cynarin has no significant effect on VP24 ISRE inhibition (Fig. 4E) while quercetin reverts VP24 inhibition in a dose-dependent manner (Fig. 4F).

3.4. Cynarin reverts the EBOV VP35 block in IFN-β stimulated genes production

As a next step, to visualize the cynarin effect at a cellular level, we performed an immunofluorescence assay. HEK 293T cells were transfected with FLAG-VP35 and stimulated with vRNA in presence or in absence of 11 μM cynarin, followed by immunostaining to for the IRF3 phosphorylated at S396 (Fig. 5). Results showed that phosphorylation and nuclear localization of activated IRF3 upon vRNA stimulation (Fig. 5A) still occurred in presence of cynarin (Fig. 5B). The total block of activation and nuclear localization of phosphorylated IRF3 caused by VP35 (Fig. 5C) was reverted in presence of cynarin (Fig. 5D), confirming

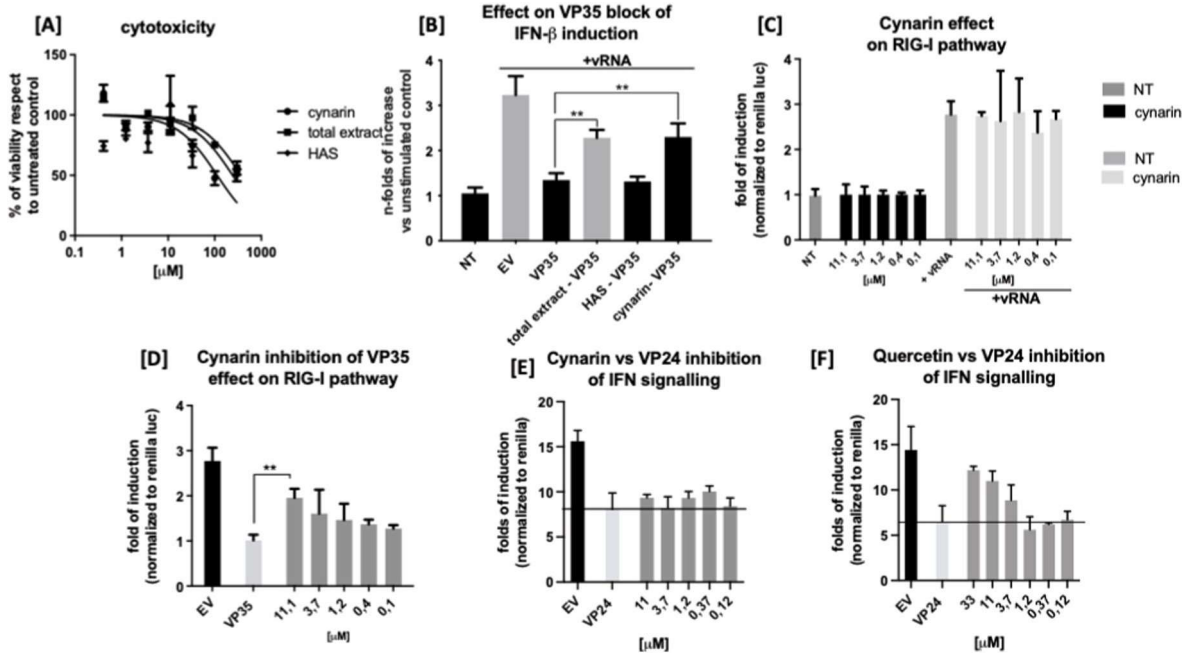

Fig. 4. Effect on the IFN promoter activation with or without EBOV VP35.
[A]. HEK293T cell viability in the presence of the selected compounds. Results were expressed in percentage of cell viability over the untreated samples. [B] Effect of selected substances on VP35 inhibition of the RIG-I pathway using 10 μg/ml total extract, 10 μM cynarin and 77 μM HAS. [C] Effect of cynarin on the RIG-I pathway in the absence of VP35. [D] Effect of cynarin on VP35 inhibition of the RIG-I pathway [E] Effect of cynarin on VP24 inhibition of the IFN signalling, [F] Effect of quercetin on VP24 inhibition of the IFN signalling Results were expressed in folds of induction over unstimulated control transfected with the empty vector, and plotted in mean plus standard deviation of two independent experiments on triplicate, with GraphPad Prism 6.01. *P < 0.05 and **P < 0.01, two-tailed unpaired Student's t-test, n = 2.

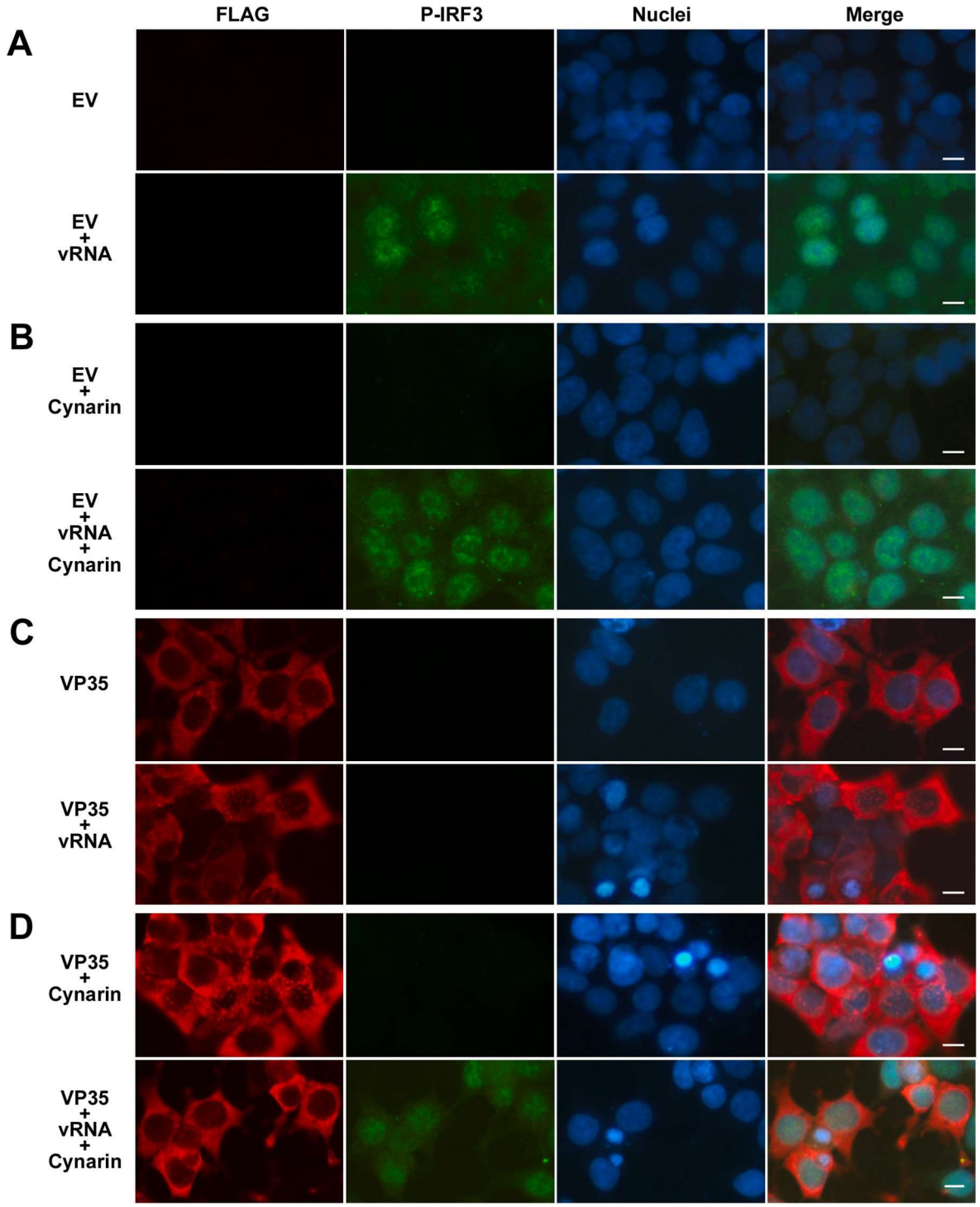

Fig. 5. Effect of cynarin on VP35 inhibition of IRF-3 phosphorylation.
Immunofluorescence of HEK293T cells [A] cotrasfected with 1 μg/well of empty vector (EV) not stimulated (row 1) or stimulated with 1 μg/mL vRNA (row 2) for 24 h, [B] cotrasfected with 1 μg/well of empty vector (EV) not stimulated (row 1) or stimulated with 1 μg/mL vRNA (row 2) and treated with 11 μM cynarin for 24 h, [C] cotrasfected with 1 μg/well of FLAG-VP35 not stimulated (row 1) or stimulated 1 μg/mL with vRNA (row 2) for 24 h, [D] cotrasfected with 1 μg/well of FLAG-VP35 not stimulated (row 1) or stimulated with 1 μg/mL vRNA (row 2) and treated with 11 μM cynarin for 24 h. Nuclei are stained in blue, FLAG-VP35 is stained in red, and S396 phospho IRF 3 is stained in green. Images were acquired at 40× magnification. Scale bar = 10 μm. . (For interpretation of the references to colour in this figure legend, the reader is referred to the Web version of this article.)

the effect of cynarin on the RIG-I pathway. In order to determine if the effect of cynarin had a consequence on the expression of IFN stimulated genes (ISGs), we analyzed the expression of two common ISGs, ISG15 and OAS2′5′, by RT-qPCR, in absence and in presence of VP35, in cells untreated or treated with 11 μM cynarin (Fig. 6A and B). Results showed that VP35 inhibited over 63% of ISG15 expression (Fig. 6A) and that in the presence of cynarin such inhibition was significantly reverted (p value = 0,011). Interestingly, the treatment of unstimulated samples with cynarin reduced the basal level of ISG15 expression by 24%, while in stimulated conditions the difference between untreated and treated

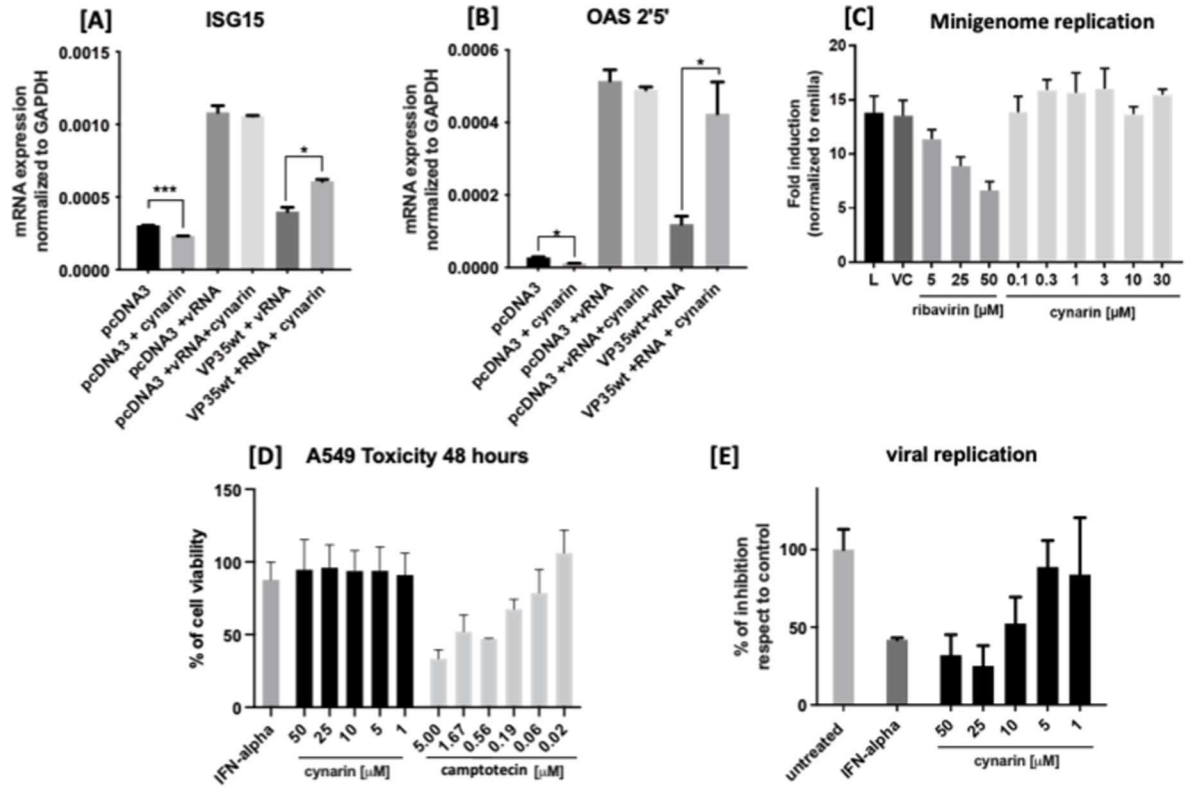

Fig. 6. [A] Effect of cynarin on VP35 inhibition of ISG15 mRNA expression. [B] Effect of cynarin on VP35 inhibition of OAS 2′5′ mRNA expression. Results are shown as fold inductions of ISG15 mRNA expression in vRNA stimulated over not stimulated cells. Error bars indicate the mean ± SD of two independent experiments. *P < 0.05 and **P < 0.01, two-tailed unpaired Student's t-test, n = 2. **[C] Effect of cynarin on VP35 minigenome replication. [D] Effect of cynarin A549 cell viability at 48 h. MTT assay** Data (mean ± SD, N = 2 experiments in triplicate) **[E] Effect of cynarin on EBOV infection.** Data (mean ± SD, N = 2 experiments in duplicate) are percentages of GP-positive cells.

samples was not significant. Similarly, VP35 reduced OAS2′ 5′ expres- sion by over70% and cynarin reverted such inhibition restoring OAS2′ 5′ expression up to 82% of the stimulated control (p value = 0,0411) (Fig. 6B). In addition, in this case treatment of unstimulated samples with cynarin reduced the basal level of ISG15 expression, while in stimulated conditions the difference between untreated and treated samples was not significant.

Overall, these data indicate that the reversion of VP35 inhibition of ISG expression was strictly VP35 dependent. To determine whether VP35 polymerase cofactor activity was affected, cynarin was further tested in an EBOV minigenome replication assay. Using the RNA- dependent RNA polymerase inhibitor Ribavirin as a positive control, cynarin showed no effect on EBOV minigenome activity (Fig. 6C).

3.5. *Cynarin inhibits EBOV infection*

We next sought to evaluate the potential antiviral effects of the cynarin against the authentic EBOV derived from the 2014 West Africa outbreak. After assessing by MTT assay that no significant cytotoxicity was observed in A549 cells (Fig. 6D), a panel of different concentrations of compound was combined with viral suspension and inoculated on target cells. At 48 h post-inoculation, infected cells were identified by immunofluorescence staining using an anti-EBOV glycoprotein (GP) antibody (Rosenstierne et al., 2016). As a positive control for viral infection inhibition 2000 IU/mL IFN-α was used. In this experimental setting, the treatment with IFN-α reduced the amount of infected cells to roughly 42% in comparison to the untreated cells, while cynarin reduced the number of infected cells in a dose-dependent manner with an EC_{50} value of 9.1 μM (Fig. 6E).

4. Discussion

In the need of finding agents able to block EBOV replication, VP35 has emerged as an attractive target for drug development (Fanunza et al., 2019; Paulis et al., 2021; Woolsey et al., 2019). In the present study we applied a recently developed fluorescence-based assay (Daino et al., 2018) to identify new ligands able to inhibit the interaction be- tween recombinant full-length VP35 and dsRNA. Extracts from *Ono- pordum illyricum*, a plant previously investigated for antibacterial and antiviral activities (Bruno et al., 2011; Sanna et al., 2018), were screened, identifying cynarin as an inhibitor of dsRNA-VP35 binding, with an IC_{50} value of 8.5 μM, in the same order of magnitude of the previously identified flavonol myricetin (Daino et al., 2018). Similar to myricetin, cynarin was shown to interact with EBOV VP35 IID. Docking experiments highlighted that cynarin could bind the end-capping site of VP35. In particular, analyzing the putative binding mode, the complex ligand-protein was shown to be stabilized by several hydrogen bonds with the backbone of Ala-238, Ile-340 and Lys-339 and with the side chain of Arg-312 and Lys-309 (Fig. 3B). The binding-mode proposed present similarities with the myricetin binding such as the interaction with Ile-340 (Daino et al., 2018).

Interestingly, some residues, such as Lys-309, Arg-312, Lys-339, are important and conserved residues inside the so called "basic patch" area that was previously shown to diminish dsRNA binding (Leung et al., 2010b).

Of importance, such cynarin binding to VP35 leads to the block of its IFN antagonism effect but does not affect its polymerase cofactor ac- tivity. It is worth to note that the high induction of ISG15 in response to IFN stimulation suggests an important role for ISG15 in antiviral defense and, in fact, ISG15 has been demonstrated to have a broad antiviral effect including suppression of EBOV viral particles budding (Skaug and

Chen, 2010). For this reason ISG15 has been used as marker for IFN stimulation in a number of studies (Au et al., 1995; Loeb and Haas, 1992; Reich et al., 1987). Considering the possible implication of VP35-IID in adaptive and innate cell-mediated responses (Lubaki et al., 2016), it is possible to hypothesize a positive effect of Cynarin on the restoration of efficient B and T cell responses during EBOV infection. Moreover, Cynarin has been shown to exert mild immunosuppressive effects, by hampering T-cell IL-2 release with limited side effects, and it has been proposed to bring benefit in suppressing patients' immune hyper-reaction (Dong et al., 2009). Taking into account that IL-2 levels has been reported as significantly increased in EVD fatalities compared to survivors and controls (Villinger et al., 1999), it is possible to spec- ulate that Cynarin modulating effects on cytokines could possibly syn- ergize whit the restoration of the innate immune response at the early stages of EBOV infection, containing the cytokine storm, while its contribution could be questionable in the late stages of infection, char- acterized by a massive lymphopenia since Cynarin inhibits specific interaction between CD28 and CD80 from APCs (Dong et al., 2009).

The ability of cynarin to inhibit EBOV replication is comparable in terms of potency of inhibition to the one showed by the immune-stimulant Nitazoxanide (EC_{50} 6 μM) (Jasenosky et al., 2019), but its potency is higher than the NP-VP35 interaction inhibitor GA017, which blocked EBOV minigenome replication with an EC_{50} value of 50 μM (Brown et al., 2014), and of the RdRp inhibitor Favipiravir (EC_{50} = 67 μM) (Oestereich et al., 2014), while lower than the other RdRp inhibitor Brincidofovir (CMX001) (EC_{50} = 120 nM to 1.3 μM) (McMullan et al., 2016).

Overall, the present data indicate that cynarin is a potent inhibitor of EBOV replication, effectively targeting VP35 IFN antagonism, although our data indicate that cynarin blocks VP35 inhibition of IRF-3 activa- tion. Further studies are certainly warranted to evaluate the possibility that cynarin may also inhibit the interaction between EBOV VP35 and other cellular components of the RIG-I pathway (Guito et al., 2017). These results can also be extended by development of cynarin de- rivatives with more potent anti-VP35 activity to further steps towards the discovery of more anti-EBOV therapeutics.

Author contributions

AC, EF, GLD, AF, CS, LZ, MJ carried out the experiments, SD per- formed the docking simulations and analyzed the data. AC, LZ, SPR, SC, CS, DR, OTS, MA, and MQ interpreted the results outcomes, ET devised, conceived and designed the project. The manuscript was written through contributions of all authors and all authors have given approval to the final version of the manuscript.

Declaration of competing interestsCOI

The authors declare that they have no known competing financial interests or personal relationships that could have appeared to influence the work reported in this paper.

Acknowledgments

A.C., S.D. and E.T FDS2019 EBOV CUPF72F20000270007.

References

Au, W.C., Moore, P.A., Lowther, W., Juang, Y.T., Pitha, P.M., 1995. Identification of a member of the interferon regulatory factor family that binds to the interferon-stimulated response element and activates expression of interferon-induced genes. Proc. Natl. Acad. Sci. U. S. A. 92, 11657–11661. https://doi.org/10.1073/pnas.92.25.11657.

Bharaj, P., Atkins, C., Luthra, P., Giraldo, M.I., Dawes, B.E., Miorin, L., Johnson, J.R., Krogan, N.J., Basler, C.F., Freiberg, A.N., Rajsbaum, R., 2017. The host E3-ubiquitin ligase TRIM6 ubiquitinates the ebola virus VP35 protein and promotes virus replication. J. Virol. 91 https://doi.org/10.1128/jvi.00833-17 e00833-17.

Binning, J.M., Wang, T., Luthra, P., Shabman, R.S., Borek, D.M., Liu, G., Xu, W., Leung, D.W., Basler, C.F., Amarasinghe, G.K., 2013. Development of RNA Aptamers Targeting Ebola Virus VP35.

Brown, C.S., Lee, M.S., Leung, D.W., Wang, T., Xu, W., Luthra, P., Anantpadma, M., Shabman, R.S., Melito, L.M., MacMillan, K.S., Borek, D.M., Otwinowski, Z., Ramanan, P., Stubbs, A.J., Peterson, D.S., Binning, J.M., Tonelli, M., Olson, M.A., Davey, R.A., Ready, J.M., Basler, C.F., Amarasinghe, G.K., 2014. In silico derived small molecules bind the filovirus VP35 protein and inhibit its polymerase cofactor activity. J. Mol. Biol. 426, 2045–2058. https://doi.org/10.1016/j.jmb.2014.01.010.

Bruno, M., Maggio, A., Rosselli, S., Safder, M., Bancheva, S., 2011. The metabolites of the genus Onopordum (asteraceae): chemistry and biological properties. Curr. Org. Chem. 15, 888–927. https://doi.org/10.2174/138527211794518880.

Cannas, V., Daino, G.L., Corona, A., Esposito, F., Tramontano, E., 2015. A luciferase reporter gene assay to measure ebola virus viral protein 35-associated inhibition of double-stranded RNA-stimulated, retinoic acid-inducible gene 1-mediated induction of interferon β. J. Infect. Dis. 212, S277–S281. https://doi.org/10.1093/infdis/jiv214.

Cardenas, W.B., Loo, Y.-M.Y., Gale, M., Hartman, A.L., Kimberlin, C.R., Martinez-Sobrido, L., Saphire, E.O., Basler, C.F., 2006. Ebola virus VP35 protein binds double-stranded RNA and inhibits alpha/beta interferon production induced by RIG-I signaling. J. Virol. 80, 5168–5178. https://doi.org/10.1128/JVI.02199-05.

Chang, T.-H., Kubota, T., Matsuoka, M., Jones, S., Bradfute, S.B., Bray, M., Ozato, K., 2009. Ebola Zaire virus blocks type I interferon production by exploiting the host SUMO modification machinery. PLoS Pathog. 5, e1000493 https://doi.org/10.1371/journal.ppat.1000493.

Cho, A.E., Guallar, V., Berne, B.J., Friesner, R., 2005. Importance of accurate charges in molecular docking: quantum mechanical/molecular mechanical (QM/MM) approach. J. Comput. Chem. 26, 915–931. https://doi.org/10.1002/jcc.20222.

Daino, G.L., Frau, A., Sanna, C., Rigano, D., Distinto, S., Madau, V., Esposito, F., Fanunza, E., Bianco, G., Taglialatela-Scafati, O., Zinzula, L., Maccioni, E., Corona, A., Tramontano, E., 2018. Identification of myricetin as an ebola virus VP35-double-stranded RNA interaction inhibitor through a novel fluorescence-based assay. Biochemistry 57, 6367–6378. https://doi.org/10.1021/acs.biochem.8b00892.

Di Palma, F., Daino, G.L., Ramaswamy, V.K., Corona, A., Frau, A., Fanunza, E., Vargiu, A. V., Tramontano, E., Ruggerone, P., 2019. Relevance of Ebola virus VP35 homo-dimerization on the type I interferon cascade inhibition. Antivir. Chem. Chemother. 27, 1–13. https://doi.org/10.1177/2040206619889220.

Dong, G.C., Chuang, P.H., Chang, K.C., Jan, P.S., Hwang, P.I., Wu, H. Bin, Yi, M., Zhou, H.X., Chen, H.M., 2009. Blocking effect of an immuno-suppressive agent, cynarin, on CD28 of T-cell receptor. Pharm. Res. 26, 375–381. https://doi.org/10.1007/s11095-008-9754-5.

Fanunza, E., Frau, A., Corona, A., Tramontano, E., 2018a. Insights into ebola virus VP35 and VP24 interferon inhibitory functions and their initial exploitation as drug targets elisa. Infect. Disord. - Drug Targets 19, 1–12. https://doi.org/10.2174/1871526519666181123145540.

Fanunza, E., Frau, A., Sgarbanti, M., Orsatti, R., Corona, A., Tramontano, E., 2018b. Development and validation of a novel dual luciferase reporter gene assay to quantify ebola virus VP24 inhibition of IFN signaling. Viruses 10. https://doi.org/10.3390/v10020098.

Fanunza, E., Frau, A., Corona, A., Tramontano, E., 2019. Antiviral Agents against Ebola Virus Infection: Repositioning Old Drugs and Finding Novel Small Molecules, ANNUAL REPORTS IN MEDICINAL CHEMISTRY. https://doi.org/10.1016/bs.armc.2018.08.004.

Fanunza, E., Iampietro, M., Distinto, S., Corona, A., Quartu, M., Maccioni, E., Horvat, B., Tramontano, E., 2020. Quercetin blocks Ebola Virus infection by counteracting the VP24 Interferon inhibitory function. Antimicrob. Agents Chemother. 64, e00530–550. https://doi.org/10.1128/AAC.00530-20.

Fda, 2020. Drug Trials Snapshots: INMAZEB | FDA. FDA [WWW Document]. https://www.fda.gov/drugs/drug-approvals-and-databases/drug-trials-snapshots-inmazeb. accessed 12.23.20.

Flego, M., Frau, A., Accardi, L., Mallano, A., Ascione, A., Gellini, M., Fanunza, E., Vella, S., Di Bonito, P., Tramontano, E., 2019. Intracellular human antibody fragments recognizing the VP35 protein of Zaire Ebola filovirus inhibit the protein activity. BMC Biotechnol. 19, 64. https://doi.org/10.1186/s12896-019-0554-2.

Friesner, R.A., Murphy, R.B., Repasky, M.P., Frye, L.L., Greenwood, J.R., Halgren, T.A., Sanschagrin, P.C., Mainz, D.T., Friesner, R.A., Murphy, R.B., Repasky, M.P., Frye, L. L., Greenwood, J.R., Halgren, T.A., Sanschagrin, P.C., Mainz, D.T., Friesner, R.A., Murphy, R.B., Repasky, M.P., Frye, L.L., Greenwood, J.R., Halgren, T.A., Sanschagrin, P.C., Mainz, D.T., 2006. Extra precision glide: docking and scoring incorporating a model of hydrophobic enclosure for protein-ligand complexes. J. Med. Chem. 49, 6177–6196. https://doi.org/10.1021/jm051256o.

Gire, S.K., Goba, A., Andersen, K.G., Sealfon, R.S.G., Park, D.J., Kanneh, L., Jalloh, S., Momoh, M., Fullah, M., Dudas, G., Wohl, S., Moses, L.M., Yozwiak, N.L., Winnicki, S., Matranga, C.B., Malboeuf, C.M., Qu, J., Gladden, A.D., Schaffner, S.F., Yang, X., Jiang, P.P., Nekoui, M., Colubri, A., Coomber, M.R., Fonnie, M., Moigboi, A., Gbakie, M., Kamara, F.K., Tucker, V., Konuwa, E., Saffa, S., Sellu, J., Jalloh, A.A., Kovoma, A., Koninga, J., Mustapha, I., Kargbo, K., Foday, M., Yillah, M., Kanneh, F., Robert, W., Massally, J.L.B., Chapman, S.B., Bochicchio, J., Murphy, C., Nusbaum, C., Young, S., Birren, B.W., Grant, D.S., Scheiffelin, J.S., Lander, E.S., Happi, C., Gevao, S.M., Gnirke, A., Rambaut, A., Garry, R.F., Khan, S.H., Sabeti, P.C., 2014. Genomic surveillance elucidates Ebola virus origin and transmission during the 2014 outbreak. Science (80-) 1369–1372. https://doi.org/10.1126/science.1259657.

Glanzer, J.G., Byrne, B.M., McCoy, A.M., James, B.J., Frank, J.D., Oakley, G.G., 2016. In silico and in vitro methods to identify ebola virus VP35-dsRNA inhibitors. Bioorg. Med. Chem. 24 (21), 5388–5392. https://doi.org/10.1016/j.bmc.2016.08.065.

Groseth, A., Charton, J.E., Sauerborn, M., Feldmann, F., Jones, S.M., Hoenen, T., Feldmann, H., 2009. The Ebola virus ribonucleoprotein complex: a novel VP30-L interaction identified. Virus Res. 140, 8–14. https://doi.org/10.1016/j.virusres.2008.10.017.

Guito, J.C., Albarin˜o, C.G., Chakrabarti, A.K., Towner, J.S., 2017. Novel activities by ebolavirus and marburgvirus interferon antagonists revealed using a standardized in vitro reporter system. Virology 501, 147–165. https://doi.org/10.1016/j.virol.2016.11.015.

Haasnoot, J., De Vries, W., Geutjes, E.J., Prins, M., De Haan, P., Berkhout, B., 2007. The ebola virus VP35 protein is a suppressor of RNA silencing. PLoS Pathog. 3 https://doi.org/10.1371/journal.ppat.0030086, 0794–0803.

Halgren, T.A., 1996. Merck molecular force field. III. Molecular geometries and vibrational frequencies for MMFF94. J. Comput. Chem. 17, 553–586. https://doi.org/10.1002/(SICI)1096-987X(199604)17:5/6<553:AID-JCC3>3.0.CO;2-T.

Hasel, W., Hendrickson, T.F., Still, W.C., 1988. A rapid approximation to the solvent accessible surface areas of atoms. Tetrahedron Comput. Methodol. 1, 103–116. https://doi.org/10.1016/0898-5529(88)90015-2.

Iversen, P.L., Warren, T.K., Wells, J.B., Garza, N.L., Mourich, D.V., Welch, L.S., Panchal, R.G., Bavari, S., 2012. Discovery and early development of AVI-7537 and AVI-7288 for the treatment of Ebola virus and Marburg virus infections. Viruses 4, 2806–2830. https://doi.org/10.3390/v4112806.

Jasenosky, L.D., Cadena, C., Mire, C.E., Borisevich, V., Haridas, V., Ranjbar, S., Nambu, A., Bavari, S., Soloveva, V., Sadukhan, S., Cassell, G.H., Geisbert, T.W., Hur, S., Goldfeld, A.E., 2019. The FDA-approved oral drug Nitazoxanide amplifies host antiviral responses and inhibits ebola virus. iScience 19, 1279–1290. https://doi.org/10.1016/j.isci.2019.07.003.

Johnson, K.M., Lange, J.V., Webb, p.A., Murphy, F.A., 1977. Isolation and partial characterisation of a new virus causing acute haemorrhagic fever in Zaire. Lancet 309, 569–571.

Kimberlin, C.R., Bornholdt, Z.A., Li, S., Woods, V.L., MacRae, I.J., Saphire, E.O., 2010. Ebolavirus VP35 uses a bimodal strategy to bind dsRNA for innate immune suppression. Proc. Natl. Acad. Sci. Unit. States Am. 107, 314–319. https://doi.org/10.1073/pnas.0910547107.

Kirchdoerfer, R.N.N., Abelson, D.M.M., Li, S., Wood, M.R.R., Saphire, E.O.O., 2015. Assembly of the ebola virus nucleoprotein from a chaperoned VP35 complex. Cell Rep. 12, 140–149. https://doi.org/10.1016/j.celrep.2015.06.003.

Le Sage, V., Cinti, A., McCarthy, S., Amorim, R., Rao, S., Daino, G.L., Tramontano, E., Branch, D.R., Mouland, A.J., 2017. Ebola virus VP35 blocks stress granule assembly. Virology 502, 73–83. https://doi.org/10.1016/j.virol.2016.12.012.

Leung, D.W., Ginder, N.D., Fulton, D.B., Nix, J., Basler, C.F., Honzatko, R.B., Amarasinghe, G.K., 2009. Structure of the Ebola VP35 interferon inhibitory domain. Proc. Natl. Acad. Sci. U. S. A. 106, 411–416. https://doi.org/10.1073/pnas.0807854106.

Leung, D.W., Prins, K.C., Basler, C.F., Amarasinghe, G.K., 2010a. Ebolavirus VP35 is a multifunctional virulence factor. Virulence 1, 526–531. https://doi.org/10.4161/viru.1.6.12984.

Leung, D.W., Prins, K.C., Borek, D.M., Farahbakhsh, M., Tufariello, J.M., Ramanan, P., Nix, J.C., Helgeson, L.A., Otwinowski, Z., Honzatko, R.B., Basler, C.F., Amarasinghe, G.K., 2010b. Structural basis for dsRNA recognition and interferon antagonism by Ebola VP35. Nat. Struct. Mol. Biol. 17, 165–172. https://doi.org/10.1038/nsmb.1765.

Leung, D.W., Shabman, R.S., Farahbakhsh, M., Prins, K.C., Borek, D.M., Wang, T., Mühlberger, E., Basler, C.F., Amarasinghe, G.K., 2010c. Structural and functional characterization of Reston Ebola virus VP35 interferon inhibitory domain. J. Mol. Biol. 399, 347–357. https://doi.org/10.1016/j.jmb.2010.04.022.

Leung, D.W., Borek, D., Luthra, P., Binning, J.M., Anantpadma, M., Liu, G., Harvey, I.B., Su, Z., Endlich-Frazier, A., Pan, J., Shabman, R.S., Chiu, W., Davey, R.A., Otwinowski, Z., Basler, C.F., Amarasinghe, G.K., 2015. An intrinsically disordered peptide from ebola virus VP35 controls viral RNA synthesis by modulating nucleoprotein-RNA interactions. Cell Rep. 11, 376–389. https://doi.org/10.1016/j.celrep.2015.03.034.

Loeb, K.R., Haas, A.L., 1992. The interferon-inducible 15-kDa ubiquitin homolog conjugates to intracellular proteins. J. Biol. Chem. 267, 7806–7813.

Lubaki, N.M., Younan, P., Santos, R.I., Meyer, M., Iampietro, M., Koup, R.A., Bukreyev, A., 2016. The ebola interferon inhibiting domains attenuate and dysregulate cell-mediated immune responses. PLoS Pathog. 12, 1–34. https://doi.org/10.1371/journal.ppat.1006031.

Luthra, P., Ramanan, P., Mire, C.E., Weisend, C., Tsuda, Y., Yen, B., Liu, G., Leung, D.W., Geisbert, T.W., Ebihara, H., Amarasinghe, G.K., Basler, C.F., 2013. Mutual antagonism between the ebola virus VP35 protein and the RIG-I activator PACT determines infection outcome. Cell Host Microbe 14, 74–84. https://doi.org/10.1016/j.chom.2013.06.010.

Mahanty, S., Bray, M., 2004. Pathogenesis of filoviral haemorrhagic fevers. Lancet Infect. Dis. 4, 487–498. https://doi.org/10.1016/S1473-3099(04)01103-X.

Malvy, D., McElroy, A.K., de Clerck, H., Günther, S., van Griensven, J., 2019. Ebola virus disease. Lancet 393 (10174), 936–948. https://doi.org/10.1016/S0140-6736(18)33132-5.

McMullan, L.K., Flint, M., Dyall, J., Albarin˜o, C., Olinger, G.G., Foster, S., Sethna, P., Hensley, L.E., Nichol, S.T., Lanier, E.R., Spiropoulou, C.F., 2016. The lipid moiety of brincidofovir is required for in vitro antiviral activity against Ebola virus. Antivir. Res. 125, 71–78. https://doi.org/10.1016/j.antiviral.2015.10.010.

Messaoudi, I., Amarasinghe, G.K., Basler, C.F., 2015. Filovirus pathogenesis and immune evasion: insights from Ebola virus and Marburg virus. Nat. Rev. Microbiol. 13 https://doi.org/10.1038/nrmicro3524.

Mitchell, W.M., Carter, W. a, 2014. The quest for effective Ebola treatment: ebola VP35 is an evidence-based target for dsRNA drugs. Emerg. Microb. Infect. 3, e77. https://doi.org/10.1038/emi.2014.77.

Mohamadi, F., Richards, N.G.J., Guida, W.C., Liskamp, R., Lipton, M., Caufield, C., Chang, G., Hendrickson, T., Still, W.C., 1990. Macromodel—an integrated software system for modeling organic and bioorganic molecules using molecular mechanics. J. Comput. Chem. 11, 440–467. https://doi.org/10.1002/jcc.540110405.

Moller, P., Pariente, N., Klenk, H.-D.H.-D.H., Becker, S., Mo¨ller, P., Pariente, N., Klenk, H.-D.H.-D.H., Becker, S., Mo, P., Pariente, N., Klenk, H.-D.H.-D.H., Becker, S., 2005. Homo-oligomerization of Marburgvirus VP35 is essential for its function in replication and transcription. J. Virol. 79, 14876–14886. https://doi.org/10.1128/JVI.79.23.14876-14886.2005.

Mühlberger, E., Weik, M., Volchkov, V.E., Klenk, H.-D.D., Becker, S., Mu, E., Becker, S., 1999. Comparison of the transcription and replication strategies of marburg virus and Ebola virus by using artificial replication systems. J. Virol. 73, 2333–2342.

Nelson, E.V., Schmidt, K.M., Dog, S., Banadyga, L., Olejnik, J., Hume, A.J., Ryabchikova, E., Ebihara, H., Kedersha, N., Ha, T., 2016. Ebola Virus Does Not Induce Stress Granule Formation during 90, pp. 7268–7284. https://doi.org/10.1128/JVI.00459-16.

Nelson, E.V., Pacheco, J.R., Hume, A.J., Cressey, T.N., Deflub´e, L.R., Ruedas, J.B., Connor, J.H., Ebihara, H., Mühlberger, E., 2017. An RNA polymerase II-driven Ebola virus minigenome system as an advanced tool for antiviral drug screening. Antivir. Res. 146, 21–27. https://doi.org/10.1016/j.antiviral.2017.08.005.

Oestereich, L., Lüdtke, A., Wurr, S., Rieger, T., Mun˜oz-Fontela, C., Günther, S., 2014. Successful treatment of advanced Ebola virus infection with T-705 (favipiravir) in a small animal model. Antivir. Res. 105, 17–21. https://doi.org/10.1016/j.antiviral.2014.02.014.

Ollmann Saphire, E., 2020. A vaccine against ebola virus. Cell 181, 6. https://doi.org/10.1016/j.cell.2020.03.011.

Paulis, A.L., Corona, A., Tramontano, E., 2021. Inhibitors of Ebolavirus Targeting Innate Immune Evasion, 1st Ed, Annual Reports in Medicinal Chemistry. Elsevier Inc. https://doi.org/10.1016/bs.armc.2021.09.003.

Prins, K.C., Ca´rdenas, W.B., Basler, C.F., 2009. Ebola virus protein VP35 impairs the function of interferon regulatory factor-activating kinases IKKepsilon and TBK-1. J. Virol. 83, 3069–3077. https://doi.org/10.1128/JVI.01875-08.

Prins, K.C., Binning, J.M., Shabman, R.S., Leung, D.W., Amarasinghe, G.K., Basler, C.F., 2010a. Basic residues within the ebolavirus VP35 protein are required for its viral polymerase cofactor function. J. Virol. 84, 10581–10591. https://doi.org/10.1128/JVI.00925-10.

Prins, K.C., Delpeut, S., Leung, D.W., Reynard, O., Volchkova, V.A., Reid, S.P., Ramanan, P., Cardenas, W.B., Amarasinghe, G.K., Volchkov, V.E., Basler, C.F., C´ardenas, W.B., Amarasinghe, G.K., Volchkov, V.E., Basler, C.F., 2010b. No Title, vol. 84, pp. 3004–3015. https://doi.org/10.1128/JVI.02459-09.

Ramaswamy, V.K., Di Palma, F., Vargiu, A., Corona, A., Piano, D., Ruggerone, P., Zinzula, L., Tramontano, E., 2018. Insights into the homo-oligomerization properties of N-terminal coiled-coil domain of Ebola virus VP35 protein. Virus Res. 247, 61–70. https://doi.org/10.1016/j.virusres.2018.02.003.

Reich, N., Evans, B., Levy, D., Fahey, D., Knight, E., Darnell, J.E., 1987. Interferon-induced transcription of a gene encoding a 15-kDa protein depends on an upstream enhancer element. Proc. Natl. Acad. Sci. U. S. A. 84, 6394–6398. https://doi.org/10.1073/pnas.84.18.6394.

Reid, S.P., C´ardenas, W.B., Basler, C.F., 2005. Homo-oligomerization facilitates the interferon-antagonist activity of the ebolavirus VP35 protein. Virology 341, 179–189. https://doi.org/10.1016/j.virol.2005.06.044.

Rosenstierne, M.W., Karlberg, H., Bragstad, K., Lindegren, G., Stoltz, M.L., Salata, C., Kran, A.M.B., Dudman, S.G., Mirazimi, A., Fomsgaard, A., 2016. Rapid bedside inactivation of Ebola virus for safe nucleic acid tests. J. Clin. Microbiol. 54, 2521–2529. https://doi.org/10.1128/JCM.00346-16.

Salata, C., Baritussio, A., Munegato, D., Calistri, A., Ha, H.R., Bigler, L., Fabris, F., Parolin, C., Palù, G., Mirazimi, A., 2015. Amiodarone and metabolite MDEA inhibit Ebola virus infection by interfering with the viral entry process. Pathog. Dis. 73 https://doi.org/10.1093/femspd/ftv032.

Sanna, C., Rigano, D., Cortis, P., Corona, A., Ballero, M., Parolin, C., Del Vecchio, C., Chianese, G., Saccon, E., Formisano, C., Tramontano, E., Esposito, F., 2018. Onopordum illyricum L., a Mediterranean plant, as a source of anti HIV-1 compounds. Plant Biosyst. - An Int. J. Deal. with all Asp. Plant Biol. 3504, 1–8. https://doi.org/10.1080/11263504.2018.1439118.

Seesuay, W., Jittavisutthikul, S., Sae-Lim, N., Sookrung, N., Sakolvaree, Y., Chaicumpa, W., 2018a. Human transbodies that interfere with the functions of Ebola virus VP35 protein in genome replication and transcription and innate immune antagonism article. Emerg. Microb. Infect. 7 https://doi.org/10.1038/s41426-018-0031-3.

Seesuay, W., Jittavisutthikul, S., Sae-Lim, N., Sookrung, N., Sakolvaree, Y., Chaicumpa, W., 2018b. Human transbodies that interfere with the functions of Ebola virus VP35 protein in genome replication and transcription and innate immune antagonism article. Emerg. Microb. Infect. 7, 41. https://doi.org/10.1038/s41426-018-0031-3.

Shah, R., Panda, P.K., Patel, P., Panchal, H., 2015. Pharmacophore based virtual screening and molecular docking studies of inherited compounds against ebola virus receptor proteins. World J. Pharm. Pharmaceut. Sci. 4, 1268–1282.

Shu, T., Gan, T., Bai, P., Wang, X., Qian, Q., Zhou, H., Cheng, Q., Qiu, Y., Yin, L., Zhong, J., Zhou, X., 2019. Ebola virus VP35 has novel NTPase and helicase-like activities. Nucleic Acids Res. 1, 1–15. https://doi.org/10.1093/nar/gkz340.

Skaug, B., Chen, Z.J., 2010. Emerging role of ISG15 in antiviral immunity. Cell 143 (2), 187–190. https://doi.org/10.1016/j.cell.2010.09.033.

Takamatsu, Y., Kolesnikova, L., Becker, S., 2018. Ebola virus proteins NP, VP35, and VP24 are essential and sufficient to mediate nucleocapsid transport. Proc. Natl. Acad. Sci. Unit. States Am. 115, 1075–1080. https://doi.org/10.1073/pnas.1712263115.

Trott, O., Olson, A.J., 2010. Software news and update AutoDock Vina: improving the speed and accuracy of docking with a new scoring function, efficient optimization, and multithreading. J. Comput. Chem. 31, 455–461. https://doi.org/10.1002/jcc.21334.

Villinger, F., Rollin, P.E., Brar, S.S., Chikkala, N.F., Winter, J., Sundstrom, J.B., Zaki, S.R., Swanepoel, R., Ansari, A.A., Peters, C.J., 1999. Markedly elevated levels of interferon (IFN)-g, IFN-a, interleukin (IL)-2, IL-10, and tumor necrosis factor-a associated with fatal ebola virus infection cording to a previously described protocol [6-8] with primers. J. Infect. Dis. 179, 188–191.

Vivoli, M., Novak, H.R., Littlechild, J.A., Harmer, N.J., 2014. Determination of protein-ligand interactions using differential scanning fluorimetry. J. Visualized Exp. 91 https://doi.org/10.3791/51809.

Weidmann, M., Sall, A.A., Manuguerra, J.C., Koivogui, L., Adjami, A., Traore´, F.F., Hedlund, K.O., Lindegren, G., Mirazimi, A., 2011. Quantitative analysis of particles, genomes and infectious particles in supernatants of haemorrhagic fever virus cell cultures. Virol. J. 8, 81. https://doi.org/10.1186/1743-422X-8-81.

Woolsey, C., Menicucci, A.R., Cross, R.W., Luthra, P., Agans, K.N., Borisevich, V., Geisbert, J.B., Mire, C.E., Fenton, K.A., Jankeel, A., Anand, S., Ebihara, H., Geisbert, T.W., Messaoudi, I., Basler, C.F., 2019. A VP35 mutant ebola virus lacks virulence but can elicit protective immunity to wild-type virus challenge. Cell Rep. 28, 3032–3046. https://doi.org/10.1016/j.celrep.2019.08.047 e6.

World Health Organization (WHO), 2019. Ebola Virus Disease – Democratic Republic of the Congo. Disease Outbreak News: Update 20 June 2019 [WWW Document].

Zinzula, L., Esposito, F., Mühlberger, E., Trunschke, M., Conrad, D., Piano, D., Tramontano, E., 2009. Purification and functional characterization of the full length recombinant Ebola virus VP35 protein expressed in E. coli. Protein Expr. Purif. 66, 113–119. https://doi.org/10.1016/j.pep.2009.02.008.

Zinzula, L., Esposito, F., Pala, D., Tramontano, E., 2012. DsRNA binding characterization of full length recombinant wild type and mutants Zaire ebolavirus VP35. Antivir. Res. 93, 354–363. https://doi.org/10.1016/j.antiviral.2012.01.005.

Zinzula, L., Nagy, I., Orsini, M., Weyher-Stingl, E., Bracher, A., Baumeister, W., 2019. Structures of ebola and reston virus VP35 oligomerization domains and comparative biophysical characterization in all ebolavirus species. Structure 27. https://doi.org/10.1016/j.str.2018.09.009.